



# Microstructure and tribological properties of TiTaHfNbZr high entropy alloy coatings deposited on Ti–6Al–4V substrates

N. Tüten<sup>a</sup>, D. Canadinc<sup>a,b,\*</sup>, A. Motallebzadeh<sup>c</sup>, B. Bal<sup>d</sup>

<sup>a</sup> Koc University, Advanced Materials Group (AMG), Department of Mechanical Engineering, Istanbul, 34450, Turkey

<sup>b</sup> University of Illinois at Urbana-Champaign, Department of Mechanical Science and Engineering, Urbana, IL, 61801, USA

<sup>c</sup> Koc University Surface Science and Technology Center (KUYTAM), Istanbul, 34450, Turkey

<sup>d</sup> Abdullah Gül University, Department of Mechanical Engineering, Kayseri, 38080, Turkey

## ARTICLE INFO

### Keywords:

High entropy alloy  
RF magnetron sputtering  
TiTaHfNbZr  
Ti–6Al–4V  
Sliding wear

## ABSTRACT

We report on the microstructure and tribological behavior of equimolar TiTaHfNbZr high entropy alloy (HEA) thin films deposited on the biomedical Ti–6Al–4V substrates by RF magnetron sputtering. Results of nanoindentation and sliding wear experiments were evaluated along with the microstructure and topographical information obtained from scanning electron microscopy and atomic force microscopy. The findings clearly demonstrate that the TiTaHfNbZr HEA not only forms a homogenous and dense coating mechanically compatible with the Ti–6Al–4V substrates, but also provides a significantly enhanced surface protection against wear and cracking, which could prove valuable especially in long-term orthopedic implants that bear dynamic contact loading, such as in the cases of hip or knee joints.

## 1. Introduction

For the sake of a reliable and safe long-term service, metallic implant materials are required to possess some essential characteristics, such as excellent biocompatibility, high corrosion resistance, adequate mechanical properties and high wear resistance [1–3]. The Ti–6Al–4V (composed of  $\alpha + \beta$  phases) constitutes one of the most widely used metallic biomaterials employed in biomedical applications [4,5], mainly owing to its higher strength, lower stiffness and density, and better biocompatibility as compared to other metallic implant materials [6–12]. However, the literature offers studies that forward clear evidence of high levels of Ti, V and Al black debris in tissue surrounding implants subject to high wear rates, such as in the case of artificial joints [13–15]. The release of toxic V and Al ions to the surrounding tissue may result in serious health problems, such as peripheral neuropathy, osteomalacia, and Alzheimer disease [4,16]. An additional and related concern for the Ti–6Al–4V alloy is raised by its relatively poor wear resistance and high coefficient of friction [17]: during service, wear leads to formation of debris, which may cause osteolysis and produce inflammatory reactions in the surrounding tissue. Therefore, improving the wear resistance, and consequently reducing debris generation, is highly desirable, especially in the case of patients with long life expectations [18].

In order to eliminate these drawbacks of the Ti–6Al–4V alloy,

coating is commonly used, such that application of appropriate coating can significantly enhance the wear resistance and lower the coefficient of friction, preventing toxic ion release [12,19,20]. Among various coating materials, Ti matrix coatings possess similar coefficient of thermal expansion as that of the Ti–6Al–4V alloy substrate, and therefore, Ti oxide layers are commonly used for Ti–6Al–4V alloy substrates. Nevertheless, it is worth mentioning that the brittle TiO<sub>2</sub> layer is vulnerable to repeated multi-axial loads in long term applications [21,22]: the existence, formation and propagation of cracks within the brittle oxide layer gives way to the release of toxic ions (Al, V), leading to the aforementioned health problems [23,24]. In order to overcome this shortcoming, considerable research has been conducted to find alternatives to conventional coating materials and broaden the scope of utility of Ti alloys in biomedical applications [25].

In general, coatings for biomedical applications must have low modulus of elasticity, high wear and corrosion resistance within the application-specific tissue or body fluids, low coefficient of friction, excellent biocompatibility, and mechanical compatibility with the substrate they are deposited on [26]. Considering the need for satisfying these requirements all at once, application of metallic coating materials onto metallic substrates manifests itself as a viable option [27–29]. Among several candidate metallic coating materials, high entropy alloys (HEAs) have recently gained attention owing to the optimum combination of mechanical properties they offer, including

\* Corresponding author. University of Illinois at Urbana-Champaign, Department of Mechanical Science and Engineering, Urbana, IL, 61801, USA.  
E-mail address: [canadinc@illinois.edu](mailto:canadinc@illinois.edu) (D. Canadinc).

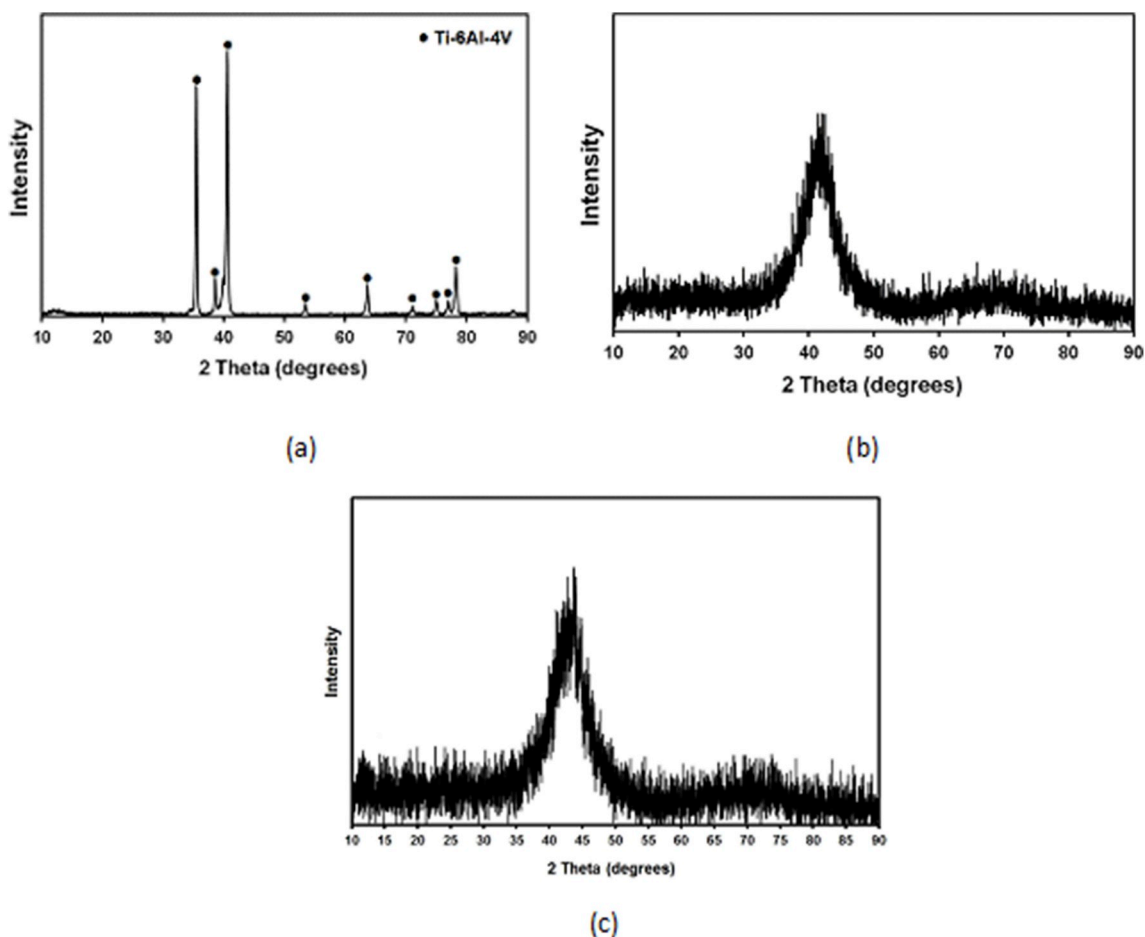


Fig. 1. XRD patterns of (a) Ti–6Al–4V substrate and TiTaHfNbZr film deposited on (b) silicon wafer and (c) Ti–6Al–4V.

high hardness, good thermal stability, and excellent wear, oxidation and corrosion resistances [30–34]. So far, several types of nitride and carbide films of HEAs have been investigated as a coating material applied onto the Ti–6Al–4V alloy and other metallic alloys: (FeCo–NiCrCuAl)N [35], (AlCrTaTiZr)N [36], (TiAlCrSiV)N [37], (AlCrMo–SiTi)N [38], (TiVCrZrHf)N [39], (TiVZrNbHf)N [40], (TiZrHfVNBa)N [41]. However, despite their significant hardness, their brittleness, limited plasticity and tendency to chipping, and more importantly, the documented Al or V ion release, constitute obstacles against their utility in implants, warranting utilization of HEA coatings composed of non-toxic elements.

One such HEA is the recently introduced equimolar TiTaHfNbZr alloy composed of individually biocompatible elements, which was coated on NiTi substrates by RF magnetron sputtering technique, and exhibited an outstanding combination of hardness and elastic modulus compatible with that of NiTi [42]. However, wear and corrosion resistances of this HEA coating have been left unattended, which constitute important considerations for coating implant materials, such as the Ti–6Al–4V alloy. In the work presented herein, we investigated the possibility of extending the utility of TiTaHfNbZr HEA as a coating deposited on the biomedical Ti–6Al–4V. For this purpose, the wear resistance of the TiTaHfNbZr HEA coatings deposited onto Ti–6Al–4V substrates by RF magnetron sputtering was investigated in correlation with the corresponding coating microstructures. Overall, the result of the present study showed that TiTaHfNbZr HEA coating has significantly reduced both coefficient of friction (CoF) and wear loss of the Ti–6Al–4V substrate, opening a venue for safer long-term utility of the Ti–6Al–4V biomedical alloy upon coating with the TiTaHfNbZr HEA.

## 2. Experimental details

The equimolar TiTaHfNbZr<sup>1</sup> HEA target was fabricated using vacuum arc melting in form of a disc with a diameter of 50.8 mm and thickness of 6.3 mm. Disc-shaped Ti–6Al–4V substrates with a diameter of 10 mm and a thickness of 2 mm were cut with electro-discharge machining. After grinding with SiC emery papers and polishing up to 0.30  $\mu\text{m}$  with alumina slurry, the samples were cleaned sequentially in acetone, isopropyl alcohol and deionized water in an ultrasonic bath. TiTaHfNbZr HEA thin films were deposited onto Ti–6Al–4V substrates and silicon wafer by RF magnetron sputtering on a Nanovak NVTS-400. Surface topography analyses and tribology experiments were carried out on the HEA thin films deposited on Ti–6Al–4V substrates. The cross-sectional inspections and XRD investigation, on the other hand, were carried out on HEA films deposited on silicon samples, such that the sample preparation was easy and the signal-to-noise ratio was improved. The deposition process was performed in an Ar atmosphere at room temperature, where the chamber base pressure was set below  $1 \times 10^{-5}$  Pa and the flow rate of Ar was kept constant at 10 standard cubic centimeters per minute (SCCM) under a power of 100 W. Prior to the deposition process, the target was pre-sputtered by Ar plasma for 10 min in order to remove the surface impurities.

The phases present in the as-deposited TiTaHfNbZr HEA film and Ti–6Al–4V substrate were investigated by X-ray diffraction (XRD) analyses were carried out on a Bruker D8 Advanced X-ray

<sup>1</sup> All constituent elements of the TiTaHfNbZr HEA were of 99.99% purity.

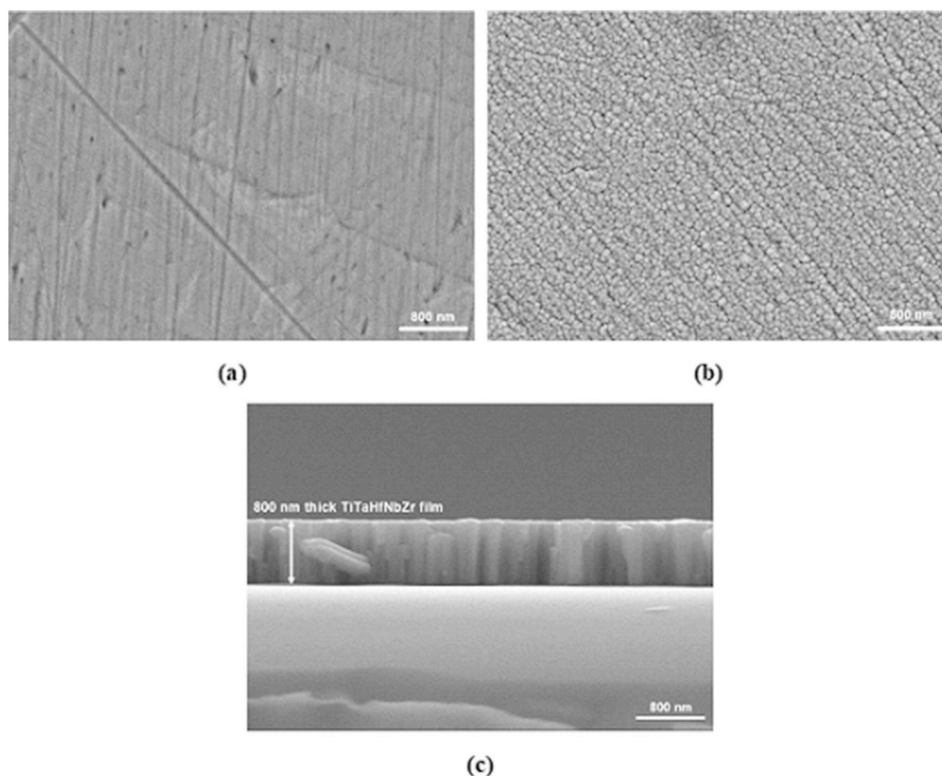


Fig. 2. SEM images of (a) Ti-6Al-4V substrate, (b) plane view of 800 nm thick TiTaHfNbZr HEA film, and (c) cross-section image of 800 nm thick TiTaHfNbZr HEA film deposited on a silicon substrate.

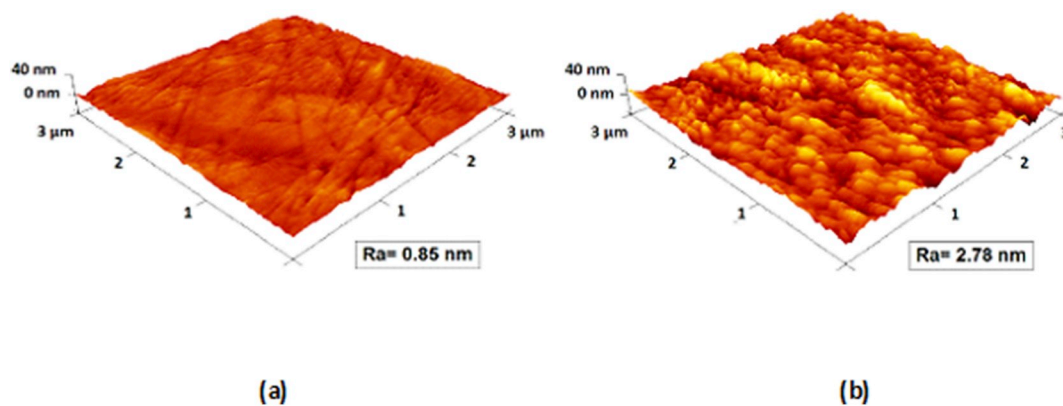


Fig. 3. AFM images and surface roughness of: (a) Ti-6Al-4V substrate, and (b) 800 nm thick TiTaHfNbZr HEA film.

diffractometer with Cu K $\alpha$  radiation operated at 40 kV and 40 mA. An incidence angle of  $4^\circ$  and an acquisition angle ranging from  $10^\circ$  to  $90^\circ$  were utilized in the grazing incidence X-ray diffraction (GIXRD) experiment with a  $0.02^\circ$  step and a scan speed of  $0.6^\circ/\text{min}$ . The morphology of sample surfaces prior to and following deposition, and the cross-section of films were explored with a Zeiss Ultra Plus scanning electron microscope (SEM), while examination of the topography and roughness of the sample surfaces were carried out with a Bruker Dimension Icon atomic force microscope (AFM) operating in the tapping mode, which enables high resolution topographic imaging of sample surfaces that are easily damaged, loosely hold to their substrate, or difficult to capture by other AFM techniques [43,44].

As for the mechanical properties, the hardness and elastic moduli of the samples were determined by nanoindentation carried out on an Agilent G200 tester employing a Berkovich diamond indenter under a continuous applied load of 3 mN. The load was applied and released under a loading/unloading rate of 0.3 mN/s with a 5 s hold at peak load

before unloading. The penetration depth of the indenter was about 1/10 of the films' thickness in order to eliminate substrate effect, and at least 15 measurements were carried out on each sample for the sake of avoiding texture effect. The average values of hardness and elastic moduli were calculated with respective standard deviations.

Sliding wear tests were performed on a tribotester (Tribotech™ Oscillating Tribotester, France) using ball-on-disc configuration in a reciprocating motion style under dry sliding condition. The experiments were carried out under applied loads of 1, 2 and 3 N at a constant sliding speed of 10 mm/s and with a stroke length of 5 mm for the total sliding distance of 30 m over the sample surfaces. A ball made of alumina ( $\text{Al}_2\text{O}_3$ ) with 6 mm diameter was used as the counterface, and the frictional force data was continuously recorded during the wear tests. Stylus type profilometer (Dektak-6M, Veeco, USA) was used to monitor the 2D profile and measure the depth and width of wear tracks developed on the surface of samples. At least eight measurements were taken from different locations on each wear track. After measuring the

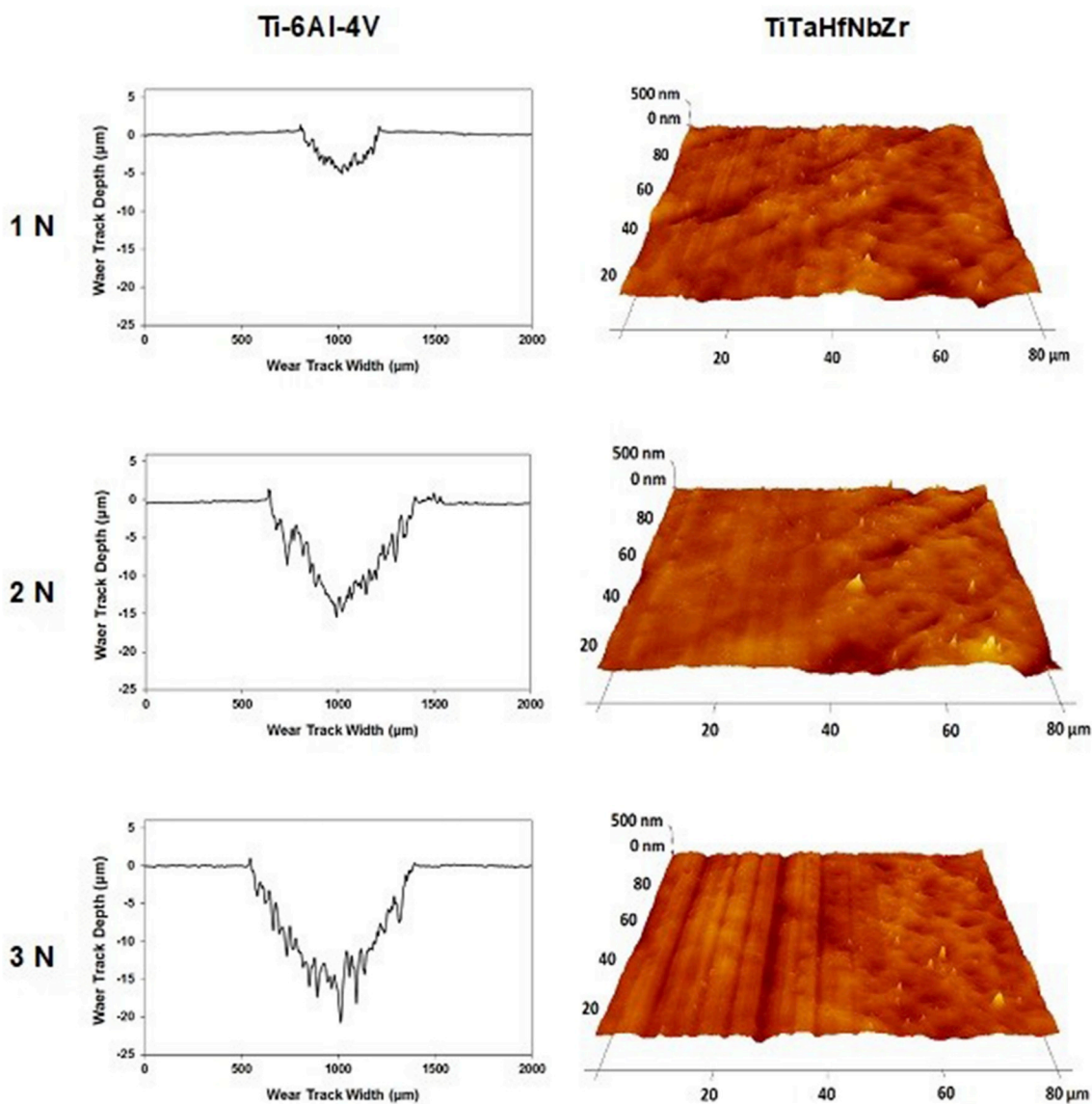


Fig. 4. 2-D profiles of the wear tracks of Ti–6Al–4V substrates and AFM images of 800 nm thick TiTaHfNbZr HEA films after the wear tests carried out under 1, 2 and 3 N loads.

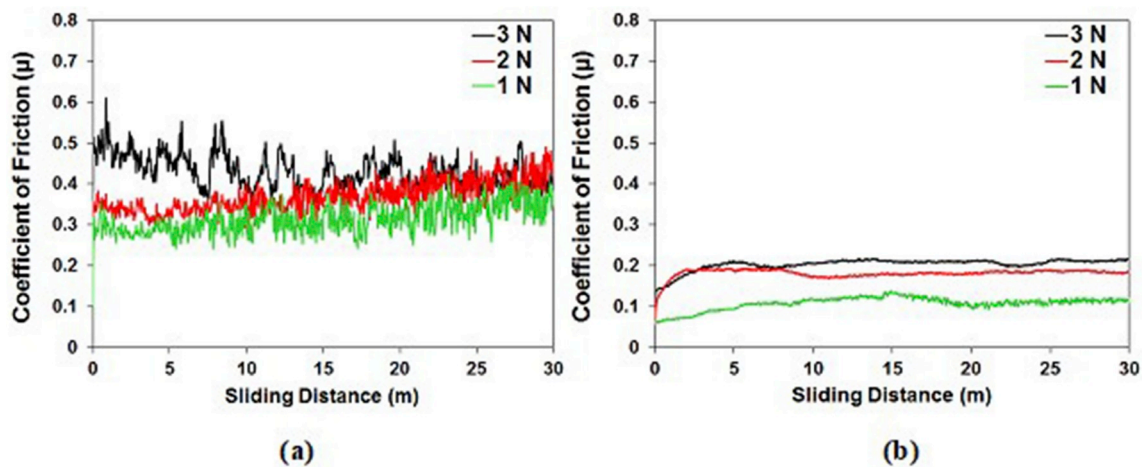


Fig. 5. Coefficient of friction profiles as a function of sliding distance for (a) Ti–6Al–4V substrate, and (b) 800 nm thick TiTaHfNbZr HEA film.

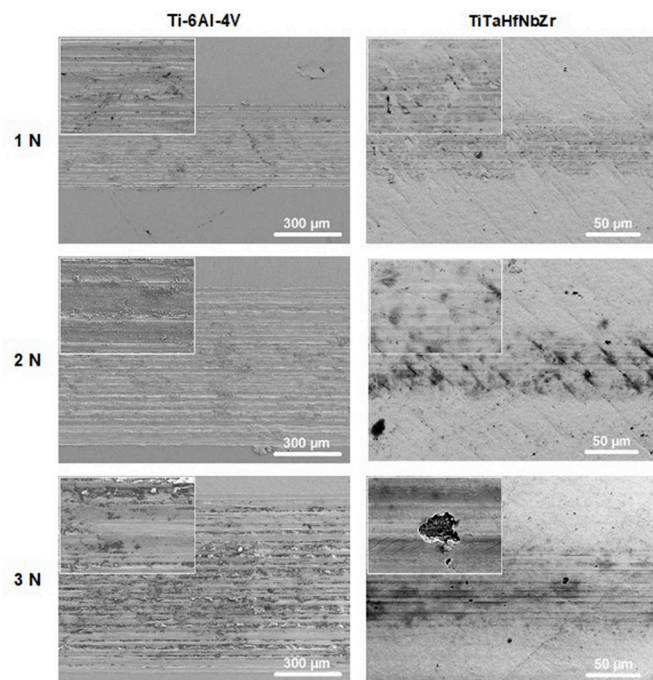


Fig. 6. The worn surface topographies of Ti–6Al–4V substrate and 800 nm thick TiTaHfNbZr HEA film.

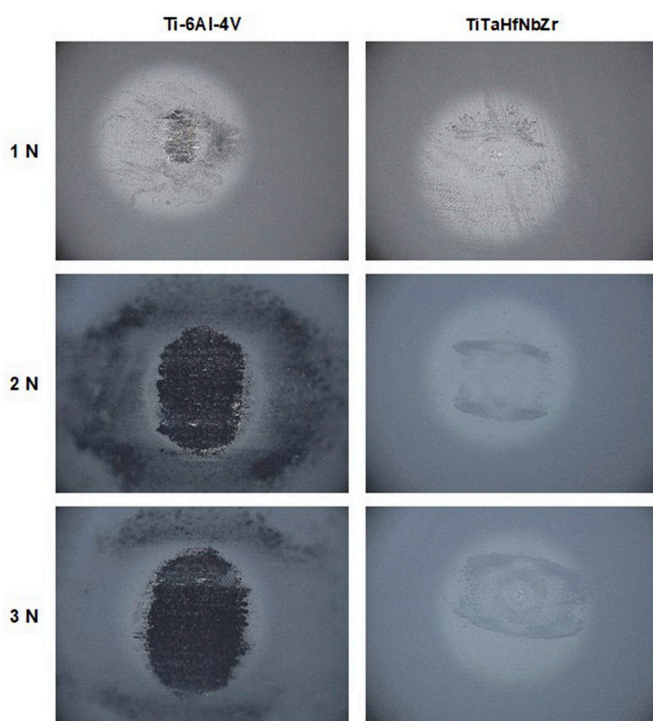


Fig. 7. Corresponding contact surface appearances of the  $\text{Al}_2\text{O}_3$  ball following the wear tests carried out under 1, 2 and 3 N loading.

average depth and width of wear tracks, the volume loss ( $\text{mm}^3$ ) was obtained by multiplying the cross-sectional area of wear track with its length. The worn surfaces of the samples were also examined by SEM and AFM.

### 3. Results and discussion

The XRD patterns of the Ti–6Al–4V alloy and the TiTaHfNbZr HEA are presented in Fig. 1(a) and (b), respectively: the TiTaHfNbZr coating exhibits a single low-intensity wide peak, indicating an amorphous structure [45], which can be explained by the rule proposed by Inoue, where the glass-forming ability can be promoted for multicomponent systems [46]. From a thermodynamics point of view, the glass-forming ability is obtained under the condition of low Gibbs free energy  $\Delta G = \Delta H_f - T\Delta S_f$  where  $\Delta H_f$  and  $\Delta S_f$  are the enthalpy and entropy, respectively. Accordingly, the low  $\Delta G$  value is obtained in the case of low  $\Delta H_f$  and large  $\Delta S_f$ , and the large  $\Delta S_f$  is expected in multi-component alloy systems since  $\Delta S_f$  is proportional to the number of the alloying elements [45–49]. Moreover, sluggish diffusion effect hinders diffusion as a result of difficulty of atom mobility in a multi-component system, which stems from higher packing density within a stack of differently-sized atoms [50]. Specifically, lower diffusion rate constitutes a reason for the higher recrystallization temperatures and activation energies of HEAs [51]. Since it is difficult to reach higher recrystallization energies within the film deposition period, formation of amorphous structure is promoted, considering the growth and even nucleation of crystalline phases are constrained [52,53].

SEM morphologies of Ti–6Al–4V substrate, and plane view and cross-section of 800 nm thick TiTaHfNbZr HEA film are presented in Fig. 2 (a), (b), and (c), respectively: white-colored and nano-sized cauliflower-like grains with sizes changing from 50 to 100 nanometers are seen on the TiTaHfNbZr HEA film deposited on Ti–6Al–4V substrate, which is consistent with findings in the literature showing that the cauliflower-like grains with sizes ranging from ten to hundreds of nanometers are typical for the most metallic films [29,47]. In addition, the SEM cross-sectional image shown in Fig. 2 (c) demonstrates that the amorphous TiTaHfNbZr HEA film obtained by RF magnetron sputtering is uniform and perfectly dense. So far several studies have revealed the remarkable hardness enhancement along with amorphous structured films [54,55]. The main strengthening mechanisms for TiTaHfNbZr HEA films were reported as small grain size and uniform amorphous structure, such that the hardening possibility of HEA films were confirmed with nanoindentation experiments.

Vickers hardness values and elastic moduli of Ti–6Al–4V substrate and TiTaHfNbZr HEA films were determined based on the loading-unloading curves obtained from nanoindentation experiments and using Oliver and Pharr method. Accordingly, the average values of the Vickers hardness and elastic modulus of the Ti–6Al–4V substrate were  $3.46 \pm 0.17$  GPa and  $115 \pm 1.4$  GPa, respectively, while the HEA films exhibited higher hardness and modulus values, namely  $12.51 \pm 0.34$  GPa and  $181.3 \pm 2.4$  GPa, respectively. In comparison to the bulk form, TiTaHfNbZr films manifested impressive enhancement in mechanical properties in terms of hardness and elastic modulus at room temperature [56–58].

The AFM surface topography and roughness of the Ti–6Al–4V substrate (Fig. 3(a)) and TiTaHfNbZr HEA film (Fig. 3(b)) demonstrated that the surface of Ti–6Al–4V substrate was rather a smooth with a

roughness of 0.85 nm, while the TiTaHfNbZr HEA coating exhibited cauliflower-like structures and its roughness was measured as 2.78 nm. In classical friction studies it is commonly accepted that the friction and wear increase with the increase in surface roughness [59–63] since rougher surfaces feature lower contact areas and apply higher contact pressures leading to higher friction and wear loss. However, for thin films under dry friction, it was shown that the coefficient of friction and wear rate generally decreased with increasing surface roughness [64]. This latter trend was also observed in the current study on TiTaHfNbZr HEA films. This inverse trend definitely needs further elaboration, yet it remains within the scope of the current work.

2-D profiles of the wear tracks formed on Ti–6Al–4V substrate and AFM images of 800 nm thick TiTaHfNbZr HEA films subjected to wear experiments are provided in Fig. 4. The depth and width of the wear tracks changed remarkably with the applied load for Ti–6Al–4V substrate. On the other hand, the wear depth was too small for TiTaHfNbZr HEA films to be detected by profilometer. Therefore, AFM images were taken following wear tests to observe the worn surfaces. Fig. 4 depicts the AFM images of surfaces of samples tested under 1, 2 and 3 N loads, including both worn and unworn zones on the same surface. The corresponding images evidence that the wear loss was negligible for TiTaHfNbZr HEA films. After determining the average depth and width of each wear track, the volumetric loss ( $\text{mm}^3$ ) calculated by multiplying the cross-sectional area of wear track with its length. Volumetric losses under 1, 2 and 3 N applied loads for Ti–6Al–4V substrate are  $7.12 \times 10^{-3}$ ,  $3.96 \times 10^{-2}$ , and  $5.75 \times 10^{-2}$ , respectively. It is well known that material volume loss by wear is highly dependent upon the hardness of tested materials and normal loads [53]. Following wear experiments; it was observed that wear loss increased with increasing normal load and decreasing hardness in the current material.

Evolution of coefficient of friction (CoF) with sliding distance are provided in Fig. 5 for applied normal loads of 1, 2 and 3 N. As a general trend, higher coefficient of friction prevailed with increasing normal load for both Ti–6Al–4V substrates and TiTaHfNbZr HEA films. The coefficient of friction was low and stable, with the value ranging from 0.1 to 0.2 for TiTaHfNbZr HEA films. On the other hand, increased wear debris generated during sliding led to oscillation and rapid increase in the coefficient of friction for Ti–6Al–4V substrate. These “third body particles” generally occur in the sliding contact and play a critical role in determining friction [65–69].

In order to acquire a comprehensive understanding of the tribological properties, wear mechanisms of the substrate and coating were analyzed using SEM. The worn surface topographies of Ti–6Al–4V substrate and 800 nm thick TiTaHfNbZr HEA film are shown in Fig. 6. The worn surfaces of Ti–6Al–4V substrate can be characterized by accumulated plastic deformation resulting from cyclic sliding contact. After increasing the normal load, plastic deformation became more dominant on the surface of Ti–6Al–4V. The sliding action of the  $\text{Al}_2\text{O}_3$  ball led to plastic deformation along with scratches in the direction of motion on the worn surfaces of the Ti–6Al–4V substrate. Diversely, for TiTaHfNbZr HEA films, plastic deformation was negligible until 3 N normal load and led to smoother surface texture. Applying 3 N caused small local ruptures on the worn surface (Fig. 6).

Corresponding contact surface appearances of the counter-face ( $\text{Al}_2\text{O}_3$  ball) for Ti–6Al–4V substrate and TiTaHfNbZr HEA films are presented in Fig. 7. The progress of wear by the plasticity dominant mechanism was accompanied by material transfer to the contact surface of the  $\text{Al}_2\text{O}_3$  ball to yield a dark colored wear scar appearance. It is clearly seen that the deposition of TiTaHfNbZr HEA films on Ti–6Al–4V substrates reduced the material removal from the coating, and therefore decreased the wear scar on the counter-face.

Overall, the current findings clearly demonstrate that the TiTaHfNbZr HEA forms a homogenous and dense coating mechanically compatible with the Ti–6Al–4V substrates it is deposited on. This coating provides a significantly enhanced surface protection against wear and cracking as compared to conventional ceramic coatings. The demonstrated tribological performance of the TiTaHfNbZr HEA could prove valuable especially in long-term orthopedic implants that bear dynamic contact loading, such as in the cases of hip or knee joints. However, the biocompatibility aspects and corrosion resistance should also be addressed prior to its biomedical utility, which constitutes the topic of our follow-up study on this material.

#### 4. Conclusion

The findings of the study presented herein demonstrate that the multi-component equimolar TiTaHfNbZr high entropy alloy (HEA) films deposited on Ti–6Al–4V substrates by RF magnetron sputtering exhibit a homogenous surface topography with a fine grained amorphous structure, providing a significant enhancement of the mechanical properties. Specifically, significant increase of hardness and elastic modulus of the surface coating led to an enhancement of the tribological properties, such as wear resistance and coefficient of friction, which dictate the suitability of coatings for biomedical applications. In summary, the current findings support that the equimolar TiTaHfNbZr HEA can serve as an effective protection against wear and cracking especially for long-term orthopedic implants.

#### Funding

This work was supported by the BAGEP Award of the Science Academy. B. Bal acknowledges the AGU-BAP [grant number FAB-2017-77].

#### References

- [1] Q. Chen, G.A. Thouas, Metallic implant biomaterials, *Mater. Sci. Eng. R Rep.* 87 (2015) 1–57, <https://doi.org/10.1016/j.mser.2014.10.001>.
- [2] D.J. Blackwood, Biomaterials: past successes and future problems, *Corrosion Rev.* 21 (2003) 97–124, <https://doi.org/10.1515/CORRREV.2003.21.2-3.97>.
- [3] M. Geetha, A.K. Singh, R. Asokamani, A.K. Gogia, Ti based biomaterials, the ultimate choice for orthopaedic implants - a review, *Prog. Mater. Sci.* 54 (2009) 397–425, <https://doi.org/10.1016/j.pmatsci.2008.06.004>.
- [4] M. Niinomi, Recent research and development in titanium alloys for biomedical applications and healthcare goods, *Sci. Technol. Adv. Mater.* 4 (2003) 445–454, <https://doi.org/10.1016/j.stam.2003.09.002>.
- [5] A. Hynowska, A. Blanquer, E. Pellicer, J. Fornell, S. Suriñach, M.D. Baró, S. González, E. Ibáñez, L. Barrios, C. Nogués, J. Sort, Novel Ti-Zr-Hf-Fe nanostructured alloy for biomedical applications, *Materials (Basel)* 6 (2013) 4930–4945, <https://doi.org/10.3390/ma6114930>.
- [6] C. Delaunay, I. Petit, I.D. Learmonth, P. Oger, P.A. Vendittoli, Metal-on-metal bearings total hip arthroplasty: the cobalt and chromium ions release concern, *Orthop. Traumatol. Surg. Res.* 96 (2010) 894–904, <https://doi.org/10.1016/j.otsr.2010.05.008>.
- [7] D.J. Langton, A.P. Sprowson, T.J. Joyce, M. Reed, I. Carluke, P. Partington, A.V.F. Nargol, Blood metal ion concentrations after hip resurfacing arthroplasty: a comparative study of articular surface replacement and birmingham hip resurfacing arthroplasties, *J. Bone Jt. Surg. - Br.* 91-B (2009) 1287–1295, <https://doi.org/10.1302/0301-620X.91B10.22308>.
- [8] R. Müller, J. Abke, E. Schnell, F. Macionczyk, U. Gbureck, R. Mehr, Z. Ruszczak, R. Kujat, C. Englert, M. Nerlich, P. Angele, Surface engineering of stainless steel materials by covalent collagen immobilization to improve implant biocompatibility, *Biomaterials* 26 (2005) 6962–6972, <https://doi.org/10.1016/j.biomaterials.2005.05.013>.
- [9] E.J. Giordani, V.A. Guimarães, T.B. Pinto, I. Ferreira, Effect of precipitates on the corrosion-fatigue crack initiation of ISO 5832-9 stainless steel biomaterial, *Int. J. Fatig.* 26 (2004) 1129–1136, <https://doi.org/10.1016/j.ijfatigue.2004.03.002>.
- [10] M. Fini, N.N. Aldini, P. Torricelli, G. Giavaresi, V. Borsari, H. Lenger, J. Bernauer, R. Giardino, R. Chiesa, A. Cigada, A new austenitic stainless steel with negligible

- nickel content: an in vitro and in vivo comparative investigation, *Biomaterials* 24 (2003) 4929–4939, [https://doi.org/10.1016/S0142-9612\(03\)00416-2](https://doi.org/10.1016/S0142-9612(03)00416-2).
- [11] R. Ebara, Corrosion fatigue crack initiation behavior of stainless steels, *Proc. Eng.* 2 (2010) 1297–1306, <https://doi.org/10.1016/j.proeng.2010.03.141>.
- [12] S.J.L. Sullivan, L.D.T. Topoleski, Surface modifications for improved wear performance in artificial joints: a review, *JOM (J. Occup. Med.)* 67 (2015) 2502–2517, <https://doi.org/10.1007/s11837-015-1543-0>.
- [13] V. Kumar, K.D. Gill, Aluminium neurotoxicity: neurobehavioural and oxidative aspects, *Arch. Toxicol.* 83 (2009) 965–978, <https://doi.org/10.1007/s00204-009-0455-6>.
- [14] V.S. de Viteri, E. Fuentes, Titanium and titanium alloys as biomaterials, *Tribol. - Fundam. Adv.* (2013), <https://doi.org/10.5772/55860>.
- [15] K. Wang, The use of titanium for medical applications in the USA, *Mater. Sci. Eng.* 213 (1996) 134–137, [https://doi.org/10.1016/0921-5093\(96\)10243-4](https://doi.org/10.1016/0921-5093(96)10243-4).
- [16] J.J. Jacobs, A.K. Skipor, L.M. Patterson, N.J. Hallab, et al., Metal release in patients who have had a primary total hip arthroplasty: a prospective controlled, longitudinal study, *J. Bone Jt. Surg.* 80 (1998) 1447–1458 [http://search.proquest.com.ezproxy.canterbury.ac.nz/docview/205150600?accountid=1449995Cnhttp://gr2tq4r79x.search.serialssolutions.com/?ctx\\_ver=Z39.88-2004&ctx\\_enc=info:ofi/enc:UTF-8&rft\\_id=info:sid/ProQ%3Ahealthcompletehell&rft\\_val\\_fmt=info:ofi/fmt:kev](http://search.proquest.com.ezproxy.canterbury.ac.nz/docview/205150600?accountid=1449995Cnhttp://gr2tq4r79x.search.serialssolutions.com/?ctx_ver=Z39.88-2004&ctx_enc=info:ofi/enc:UTF-8&rft_id=info:sid/ProQ%3Ahealthcompletehell&rft_val_fmt=info:ofi/fmt:kev).
- [17] B.D. Beake, T.W. Liskiewicz, Tribology International Comparison of nano-fretting and nano-scratch tests on biomedical materials, *Tribol. Int.* 63 (2013) 123–131, <https://doi.org/10.1016/j.triboint.2012.08.007>.
- [18] S. Bruschi, R. Bertolini, F. Medeoassi, A. Ghiotti, E. Savio, R. Shivpuri, Case study: the application of machining-conditioning to improve the wear resistance of Ti6Al4V surfaces for human hip implants, *Wear* 394–395 (2018) 134–142, <https://doi.org/10.1016/j.wear.2017.10.013>.
- [19] D.M. Mattox, *Handbook of Physical Vapor Deposition (PVD) Processing*, second ed., Elsevier Inc, Oxford, 2010.
- [20] C. Pierret, L. Maunoury, I. Monnet, S. Bouffard, A. Benyagoub, C. Grygiel, Friction and wear properties modification of Ti–6Al–4V alloy surfaces by implantation of multi-charged carbon ions, *Wear* 319 (2014) 19–26, <https://doi.org/10.1016/j.wear.2014.07.001>.
- [21] S.M. Toker, D. Canadinc, Evaluation of the biocompatibility of NiTi dental wires: a comparison of laboratory experiments and clinical conditions, *Mater. Sci. Eng. C. Mater. Biol. Appl.* 40 (2014) 142–147, <https://doi.org/10.1016/j.msec.2014.03.060>.
- [22] H. Cao, X. Liu, Activating titanium oxide coatings for orthopedic implants, *Surf. Coating. Technol.* 233 (2013) 57–64, <https://doi.org/10.1016/j.surfcoat.2013.01.043>.
- [23] C. Leyens, M. Peters, W.A. Kaysser, J. Hi, S. Iltis, *Intermetallic Ti–Al Coatings for Protection of Titanium Alloys: Oxidation and Mechanical Behavior* vol. 95, (1997).
- [24] J. Bogdan, A. Jackowska-Tracz, J. Zarzyńska, J. Pławińska-Czarnak, Chances and limitations of nanosized titanium dioxide practical application in view of its physicochemical properties, *Nanoscale Res. Lett.* 10 (2015) 1–10, <https://doi.org/10.1186/s11671-015-0753-2>.
- [25] L. Zhao, P.K. Chu, Y. Zhang, Z. Wu, Antibacterial coatings on titanium implants, *J. Biomed. Mater. Res. B Appl. Biomater.* 91 (2009) 470–480, <https://doi.org/10.1002/jbm.b.31463>.
- [26] V. Braic, M. Balaceanu, M. Braic, A. Vladescu, S. Panseri, A. Russo, Characterization of multi-principal-element (TiZrNbHfTa)N and (TiZrNbHfTa)C coatings for biomedical applications, *J. Mech. Behav. Biomed. Mater.* 10 (2012) 197–205, <https://doi.org/10.1016/j.jmbbm.2012.02.020>.
- [27] D. Pradhan, A.W. Wren, S.T. Mixture, N.P. Mellott, Investigating the structure and biocompatibility of niobium and titanium oxides as coatings for orthopedic metallic implants, *Mater. Sci. Eng. C* 58 (2016) 918–926, <https://doi.org/10.1016/j.msec.2015.09.059>.
- [28] F. Matassi, A. Botti, L. Sirleo, C. Carulli, M. Innocenti, Porous metal for orthopedic implants, *Clin. Cases Miner. Bone Metab.* 10 (2013) 111–115, <https://doi.org/10.11138/ccmbm/2013.10.2.111>.
- [29] Z. Li, K. Aik Khor, Preparation and Properties of Coatings and Thin Films on Metal Implants BT - Reference Module in Biomedical Sciences, Elsevier, 2017, <https://doi.org/10.1016/B978-0-12-801238-3.11025-6>.
- [30] K.G. Pradeep, C.C. Tasan, M.J. Yao, Y. Deng, H. Springer, D. Raabe, Non-equiatomically high entropy alloys: approach towards rapid alloy screening and property-oriented design, *Mater. Sci. Eng.* 648 (2015) 183–192, <https://doi.org/10.1016/j.msea.2015.09.010>.
- [31] Y. Zhang, T.T. Zuo, Z. Tang, M.C. Gao, K.A. Dahmen, P.K. Liaw, Z.P. Lu, Microstructures and properties of high-entropy alloys, *Prog. Mater. Sci.* 61 (2014) 1–93, <https://doi.org/10.1016/j.pmatsci.2013.10.001>.
- [32] C.-J. Tong, Y.-L. Chen, J.-W. Yeh, S.-J. Lin, S.-K. Chen, T.-T. Shun, C.-H. Tsau, S.-Y. Chang, Microstructure characterization of Al x CoCrCuFeNi high-entropy alloy system with multiprincipal elements, *Mater. Mater. Trans.* 36 (2005) 881–893, <https://doi.org/10.1007/s11661-005-0283-0>.
- [33] B. Cantor, I.T.H. Chang, P. Knight, A.J.B. Vincent, Microstructural development in equiatomic multicomponent alloys, *Mater. Sci. Eng.* 375–377 (2004) 213–218, <https://doi.org/10.1016/j.msea.2003.10.257>.
- [34] C. Huang, Y. Zhang, R. Vilar, J. Shen, Dry sliding wear behavior of laser clad TiVCrAlSi high entropy alloy coatings on Ti-6Al-4V substrate, *Mater. Des.* 41 (2012) 338–343, <https://doi.org/10.1016/j.matdes.2012.04.049>.
- [35] T.K. Chen, M.S. Wong, T.T. Shun, J.W. Yeh, Nanostructured nitride films of multi-element high-entropy alloys by reactive DC sputtering, *Surf. Coating. Technol.* 200 (2005) 1361–1365, <https://doi.org/10.1016/j.surfcoat.2005.08.081>.
- [36] C. Lai, S. Lin, J. Yeh, S. Chang, Preparation and characterization of AlCrTaTiZr multi-element nitride coatings, *Surf. Coating. Technol.* 201 (2006) 3275–3280, <https://doi.org/10.1016/j.surfcoat.2006.06.048>.
- [37] C.H. Lin, J.G. Duh, J.W. Yeh, Multi-component nitride coatings derived from Ti–Al–Cr–Si–V target in RF magnetron sputter, *Surf. Coating. Technol.* 201 (2007) 6304–6308, <https://doi.org/10.1016/j.surfcoat.2006.11.041>.
- [38] B. Ren, Z.X. Liu, L. Shi, B. Cai, M.X. Wang, Structure and properties of (AlCrMnMoNiZrB<sub>0.1</sub>)<sub>N<sub>x</sub></sub> coatings prepared by reactive DC sputtering, *Appl. Surf. Sci.* 257 (2011) 7172–7178, <https://doi.org/10.1016/j.apsusc.2011.03.083>.
- [39] H.W. Chang, P.K. Huang, A. Davison, J.W. Yeh, C.H. Tsau, C.C. Yang, Nitride films deposited from an equimolar Al-Cr-Mo-Si-Ti alloy target by reactive direct current magnetron sputtering, *Thin Solid Films* 516 (2008) 6402–6408, <https://doi.org/10.1016/j.tsf.2008.01.019>.
- [40] O.V. Sobol, A.A. Andreev, V.F. Gorban, N.A. Krapivka, V.A. Stolbovoi, I.V. Serdyuk, V.E. Fil, Reproducibility of the single phase structural state of the multielement high entropy Ti–V–Zr–Nb–Hf system and related superhard nitrides formed by the vacuum arc, *Method* 38 (2012) 616–619, <https://doi.org/10.1134/S1063785012070127>.
- [41] S.N. Grigorov, O.V. Sobol, V.M. Beresnev, I.V. Serdyuk, A.D. Pogrebnyak, D.A. Kolesnikov, U.S. Nemchenko, Tribological Characteristics of (TiZrHfV/NbTa)N Coatings Applied vol. 35, (2014), pp. 359–364, <https://doi.org/10.3103/S1068366614050067>.
- [42] A. Motallebzadeh, M.B. Yagci, E. Bedir, C.B. Aksoy, D. Canadinc, Mechanical properties of TiTaHfNbZr high-entropy alloy coatings deposited on NiTi shape memory alloy substrates, *Metall. Mater. Trans.* 49 (2018) 1992–1997, <https://doi.org/10.1007/s11661-018-4605-4>.
- [43] S.N. Magonov, V. Elings, M.H. Whangbo, Phase imaging and stiffness in tapping-mode atomic force microscopy, *Surf. Sci.* 375 (1997), [https://doi.org/10.1016/S0039-6028\(96\)01591-9](https://doi.org/10.1016/S0039-6028(96)01591-9).
- [44] H. Hölscher, AFM, tapping mode, in: B. Bhushan (Ed.), *Encycl. Nanotechnol.* Springer Netherlands, Dordrecht, 2012, p. 99, [https://doi.org/10.1007/978-90-481-9751-4\\_33](https://doi.org/10.1007/978-90-481-9751-4_33).
- [45] C.W. Tsai, S.W. Lai, K.H. Cheng, M.H. Tsai, A. Davison, C.H. Tsau, J.W. Yeh, Strong amorphization of high-entropy AlBCrSiTi nitride film, *Thin Solid Films* 520 (2012) 2613–2618, <https://doi.org/10.1016/j.tsf.2011.11.025>.
- [46] A. Inoue, High strength bulk amorphous alloys with low critical cooling rates (overview), *Mater. Trans., JIM* 36 (1995) 866–875, <https://doi.org/10.2320/matertrans1989.36.866>.
- [47] Y.S. Huang, L. Chen, H.W. Lui, M.H. Cai, J.W. Yeh, Microstructure, hardness, resistivity and thermal stability of sputtered oxide films of AlCoCrCu<sub>0.5</sub>NiFe high-entropy alloy, *Mater. Sci. Eng.* 457 (2007) 77–83, <https://doi.org/10.1016/j.msea.2006.12.001>.
- [48] M.I. Lin, M.H. Tsai, W.J. Shen, J.W. Yeh, Evolution of structure and properties of multi-component (AlCrTaTiZr)Ox films, *Thin Solid Films* 518 (2010) 2732–2737, <https://doi.org/10.1016/j.tsf.2009.10.142>.
- [49] J. Zhang, J.B. Zhu, Z.Y. Sun, J.C. Li, Preparation of amorphous coatings of AlFeCoNiCuZrV alloy by direct current magnetron sputtering method, *Asian J. Chem.* 26 (2014) 5627–5630 <http://10.055.153/ajchem.2014.18172>.
- [50] A. Inoue, Bulk amorphous alloys, in: A. Inoue, K. Hashimoto (Eds.), *Amorph. Nanocrystalline Mater. Prep. Prop. Appl.* Springer Berlin Heidelberg, Berlin, Heidelberg, 2001, pp. 1–51, [https://doi.org/10.1007/978-3-662-04426-1\\_1](https://doi.org/10.1007/978-3-662-04426-1_1).
- [51] J.W. Yeh, Recent progress in high-entropy alloys, *Ann. Chim. Sci. Des. Mater.* 31 (2006) 633–648, <https://doi.org/10.3166/acsm.31.633-648>.
- [52] G. Jin, Z. Cai, Y. Guan, X. Cui, Z. Liu, Y. Li, M. Dong, D. Zhang, High temperature wear performance of laser-cladded FeNiCoAlCu high-entropy alloy coating, *Appl. Surf. Sci.* 445 (2018) 113–122, <https://doi.org/10.1016/j.apsusc.2018.03.135>.
- [53] F.Y. Shu, L. Wu, H.Y. Zhao, S.H. Sui, L. Zhou, J. Zhang, W.X. He, P. He, B.S. Xu, Microstructure and high-temperature wear mechanism of laser cladded CoCrBFeNiSi high-entropy alloy amorphous coating, *Mater. Lett.* 211 (2018) 235–238, <https://doi.org/10.1016/j.matlet.2017.09.056>.
- [54] A.L. Greer, K.L. Rutherford, I.M. Hutchings, Wear resistance of amorphous alloys and related materials, *Int. Mater. Rev.* 47 (2002) 87–112, <https://doi.org/10.1179/095066001225001067>.
- [55] T. Zehnder, J. Patscheider, Nanocomposite TiC/a-C:H hard coatings deposited by reactive PVD, *Surf. Coating. Technol.* 133 (2000) 138–144, [https://doi.org/10.1016/S0257-8972\(00\)00888-4](https://doi.org/10.1016/S0257-8972(00)00888-4).
- [56] J. Ren, X.-B. Liu, X.-L. Lu, P.-C. Yu, G.-X. Zhu, Y. Chen, D. Xu, Microstructure and tribological properties of self-lubricating antiwear composite coating on Ti6Al4V alloy, *Surf. Eng.* 33 (2017) 20–26, <https://doi.org/10.1179/1743294415Y.0000000054>.
- [57] C. Republic, C. Republic, C. Republic, Structure and mechanical properties of

- tanbhfzrti high entropy alloy, (2015), pp. 3–8.
- [58] N. Larianovsky, A. Katz-Demyanetz, E. Eshed, M. Regev, Microstructure, tensile and creep properties of Ta<sub>20</sub>Nb<sub>20</sub>Hf<sub>20</sub>Zr<sub>20</sub>Ti<sub>20</sub> high entropy alloy, *Materials (Basel)* 10 (2017) 1–12, <https://doi.org/10.3390/ma10080883>.
- [59] J. Ren, X.-B. Liu, X.-L. Lu, P.-C. Yu, G.-X. Zhu, Y. Chen, D. Xu, Microstructure and tribological properties of self-lubricating antiwear composite coating on Ti6Al4V alloy, *Surf. Eng.* 33 (2017) 20–26, <https://doi.org/10.1179/1743294415Y.0000000054>.
- [60] N. Ravi, R. Markandeya, S.V. Joshi, Effect of substrate roughness on adhesion and tribological properties of nc-TiAlN/a-Si<sub>3</sub>N<sub>4</sub> nanocomposite coatings deposited by cathodic arc PVD process, *Surf. Eng.* 33 (2017) 7–19, <https://doi.org/10.1179/1743294415Y.0000000005>.
- [61] R. Lu, H. Zhang, Y. Mitsuya, K. Fukuzawa, S. Itoh, Influence of surface roughness and coating on the friction properties of nanometer-thick liquid lubricant films, *Wear* 319 (2014) 56–61, <https://doi.org/10.1016/j.wear.2014.07.010>.
- [62] M. Federici, C. Menapace, A. Moscatelli, S. Gialanella, G. Straffelini, Effect of roughness on the wear behavior of HVOF coatings dry sliding against a friction material, *Wear* 368–369 (2016) 326–334, <https://doi.org/10.1016/j.wear.2016.10.013>.
- [63] M.L. Rahaman, L. Zhang, M. Liu, W. Liu, Surface roughness effect on the friction and wear of bulk metallic glasses, *Wear* 332–333 (2015) 1231–1237, <https://doi.org/10.1016/j.wear.2014.11.030>.
- [64] J.A. Ogilvy, Numerical simulation of friction between contacting rough surfaces, *J. Phys. D Appl. Phys.* 24 (1991) 2098–2109, <https://doi.org/10.1088/0022-3727/24/11/030>.
- [65] N. Fillot, I. Iordanoff, Y. Berthier, Modelling third body flows with a discrete element method—a tool for understanding wear with adhesive particles, *Tribol. Int.* 40 (2007) 973–981, <https://doi.org/10.1016/j.triboint.2006.02.056>.
- [66] N. Fillot, I. Iordanoff, Y. Berthier, Wear modeling and the third body concept, *Wear* 262 (2007) 949–957, <https://doi.org/10.1016/j.wear.2006.10.011>.
- [67] H.W. Wu, Y.Y. Chen, J.H. Hornig, Contact temperature under three-body dry friction conditions, *Wear* 330–331 (2015) 85–92, <https://doi.org/10.1016/j.wear.2015.01.060>.
- [68] S. Descartes, C. Desrayaud, E. Niccolini, Y. Berthier, Presence and role of the third body in a wheel-rail contact, *Wear* 258 (2005) 1081–1090, <https://doi.org/10.1016/j.wear.2004.03.068>.
- [69] D. Majcherczak, P. Dufrenoy, Y. Berthier, M. Nait-Abdelaziz, Experimental thermal study of contact with third body, *Wear* 261 (2006) 467–476, <https://doi.org/10.1016/j.wear.2005.12.006>.